

Beyond the quasiparticle approximation: Fully self-consistent GW calculationsManuel Grumet,¹ Peitao Liu,^{1,*} Merzuk Kaltak,¹ Jiří Klimeš,^{2,3} and Georg Kresse^{1,†}¹University of Vienna, Faculty of Physics and Center for Computational Materials Science, Sensengasse 8/12, A-1090 Vienna, Austria²J. Heyrovský Institute of Physical Chemistry, Academy of Sciences of the Czech Republic, Dolejškova 3, CZ-18223 Prague 8, Czech Republic³Department of Chemical Physics and Optics, Faculty of Mathematics and Physics, Charles University, Ke Karlovu 3, CZ-12116 Prague 2, Czech Republic

(Received 23 August 2018; revised manuscript received 9 October 2018; published 29 October 2018)

We present quasiparticle (QP) energies from fully self-consistent GW (sc GW) calculations for a set of prototypical semiconductors and insulators within the framework of the projector-augmented-wave methodology. To obtain converged results, both finite basis-set corrections and k -point corrections are included, and a simple procedure is suggested to deal with the singularity of the Coulomb kernel in the long-wavelength limit, the so-called head correction. It is shown that the inclusion of the head corrections in the sc GW calculations is critical to obtain accurate QP energies with a reasonable k -point set. We first validate our implementation by presenting detailed results for the selected case of diamond, and then we discuss the converged QP energies, in particular the band gaps, for a set of gapped compounds and compare them to single-shot G_0W_0 , QP self-consistent GW , and previously available sc GW results as well as experimental results.

DOI: [10.1103/PhysRevB.98.155143](https://doi.org/10.1103/PhysRevB.98.155143)**I. INTRODUCTION**

Hedin's equations [1,2] are in principle a rigorous and exact way to calculate quasiparticle (QP) energies (electron addition or removal energies). Nevertheless, in practice the equations cannot be solved exactly due to the need to perform the calculations self-consistently and difficulties in including the vertex correction, which is defined as the functional derivative of the self-energy with respect to the external potential. Therefore, approximations are strictly required. One of the most widely used approximations is the GW approximation [1], which neglects the vertex completely. Related to this, it is furthermore common to start from orbitals determined using density functional theory (DFT) and to perform so-called single-shot G_0W_0 calculations [3–6]. This generally gives good agreement with experiments for extended, moderately correlated materials because of a cancellation of errors originating from the lack of self-consistency and the absence of vertex corrections. In order to go beyond G_0W_0 , several strategies such as the cumulant expansion [7–11], inclusion of some approximate vertex [12–15], and quantum chemistry methods like algebraic-diagrammatic construction (ADC) and equation-of-motion coupled cluster [16] have been proposed.

A problem that most single-shot Green's function based methods have in common is that some conservation laws such as energy and particle-number conservation [17,18] are violated. Due to their perturbative nature, the results also depend on the starting one-electron energies and orbitals, which are usually obtained from the solution of the Kohn-Sham (KS) equations or generalized KS schemes [19,20]. This issue can be avoided by performing the calculations self-

consistently. Eigenvalue self-consistent GW [21–23], which updates the eigenvalues either only in the Green's functions G (ev- GW_0), or both in G and the screened interactions W (ev- GW), while the orbitals remain fixed, generally improves the description of band gaps towards the experimental values as compared to G_0W_0 . Quasiparticle self-consistent GW (QP GW) removes the starting-point dependence entirely by determining an optimum effective nonlocal static exchange-correlation potential [24–27]. However, it overestimates band gaps in solids due to the underestimation of the dielectric screening in the random phase approximation (RPA) [27,28]. Self-consistent GW (sc GW) avoids the quasiparticle approximation, and the Dyson equation for the Green's function and W are solved fully self-consistently [12,13,29–34]. In addition, the self-consistent W is invariant under spatial and time translations, so conservation laws (momentum, energy, and particle-number conservation) [17,18] are satisfied in sc GW . Nevertheless, without vertex corrections, sc GW shows a significant overestimation of the bandwidth for metals and band gaps for gapped systems. Recently, there have been attempts to include the vertex in W and the self-energy for crystalline materials [12–15], showing a substantial improvement on the bandwidths, ionization potentials, and band gaps compared to sc GW . These approaches are computationally exceedingly demanding and will not be considered in this work.

Although there are already some studies that are dedicated to full sc GW calculations [12,13,29–34], they are restricted to few systems and reference results for a more extensive set of materials are still missing. The main problems in obtaining reference values for solids are threefold. First, full sc GW calculations are technically demanding. Second, the basis-set convergence for the QP energies is very slow [35–37]. Third, there is a singularity problem associated with the long-wavelength limit of the product of the Coulomb kernel and the dielectric function. Within G_0W_0 , this issue can be solved

*peitao.liu@univie.ac.at

†georg.kresse@univie.ac.at

straightforwardly using $\mathbf{k} \cdot \mathbf{p}$ perturbation theory [38–40], but this is intractable for scGW.

The goal of this paper is to obtain converged scGW QP energies for a set of semiconductors and insulators within the framework of the projector-augmented-wave (PAW) methodology. To establish reference values, we include finite basis-set corrections, as well as k -point corrections. The singularity problem in the product of the Coulomb kernel and the dielectric matrix is overcome by an extrapolation from the available results at finite \mathbf{q} . In addition to scGW results, we also report results for G_0W_0 and QPGW calculations. It should be noted that in this work, vertex corrections are not considered and therefore it is expected that our scGW results will overestimate the band gaps as compared to the experimental values.

The paper is organized as follows. In Sec. II we will detail the methodology of our scGW implementation. Particular emphasis is devoted to the extrapolation scheme that is used to solve the singularity problem of the Coulomb operator. Technical details and computational setups will be provided in Sec. III. The results will be presented and discussed in Sec. IV and summarized in Sec. V.

II. METHOD

A. Self-consistent GW

Our scGW scheme is based on our recent cubic-scaling GW implementation [41], where the polarizability and self-energy are calculated in the real-space and imaginary-time domains [42,43]. Efficient temporal discrete Fourier transformations with only a few nonuniform optimized imaginary grid points [44] and spatial fast Fourier transformations (FFT) [45] allow for fast QP calculations with a scaling that is cubic in the system size and linear in the number of k points that are used to sample the Brillouin zone. The implementation has been validated by successfully predicting QP energies of typical semiconductors, insulators, and metals as well as molecules [41,46,47]. Here, we go one step further and introduce self-consistency both in G and W . It needs to be mentioned that, for consistency, in this paper we follow almost the same notations and definitions that were used in our previous publication [41]. In the following, we present our scGW implementation in detail.

Starting from the correlated self-energy $\Sigma^c(i\omega)$ obtained from G_0W_0 [41], the new interacting Green's function $G(i\omega)$ for the next iteration is calculated in the Hartree-Fock (HF) canonical-orbital basis by the Dyson's equation

$$G(i\omega) = [i\omega + \mu - H^{\text{HF}} - \Sigma^c(i\omega)]^{-1}, \quad (1)$$

where μ is the Fermi energy and $H^{\text{HF}} = T + V_{n-e} + V_H + \Sigma^x$ is the HF Hamiltonian, with T , V_{n-e} , V_H , and Σ^x being the kinetic energy, the potential from the nuclei, the Hartree potential, and the exact exchange, respectively. Note that in this work, μ is always set to the Hartree-Fock Fermi energy, which is located at midgap between the Hartree-Fock valence band maximum (VBM) and conduction band minimum (CBM). This does not introduce any approximation since in scGW one can choose the Fermi level anywhere between the scGW VBM and CBM, which are not broadened by lifetime effects. For the materials considered in this work, this was always the case.

The interacting density matrix is then calculated in the canonical HF basis by

$$\Gamma_{ij} = \frac{1}{2\pi} \int_{-\infty}^{+\infty} d\omega G_{ij}(i\omega). \quad (2)$$

However, this integral usually diverges. To address this issue, $G(i\omega)$ is split into two parts

$$G(i\omega) = G^{\text{HF}}(i\omega) + G^c(i\omega). \quad (3)$$

Here, $G^{\text{HF}}(i\omega)$ is the HF Green's function

$$G^{\text{HF}}(i\omega) = [i\omega + \mu - H^{\text{HF}}]^{-1}, \quad (4)$$

and $G^c(i\omega)$ is the correlated part of the Green's function. Due to the splitting in Eq. (3), the density matrix includes two contributions

$$\Gamma_{ij} = \Gamma_{ij}^{\text{HF}} + \Gamma_{ij}^c, \quad (5)$$

where the calculation of the HF density matrix Γ_{ij}^{HF} is straightforward:

$$\Gamma_{ij}^{\text{HF}} = \theta(\mu - \epsilon_i^{\text{HF}}) \delta_{ij}. \quad (6)$$

Here, θ is the Heaviside step function and ϵ_i^{HF} are the eigenvalues of the HF Hamiltonian [we note again that the matrices are presented in the canonical HF basis, making $H^{\text{HF}}(i\omega)$ and $G^{\text{HF}}(i\omega)$ diagonal]. Since $\Sigma^c(i\omega)$ decays as $1/(i\omega)$ [48], $G^c(i\omega)$ decays as $1/(i\omega)^3$. The correlated contribution Γ_{ij}^c can thus be calculated accurately by exploiting quadrature rules

$$\Gamma_{ij}^c = \frac{1}{2\pi} \int_{-\infty}^{+\infty} d\omega G_{ij}^c(i\omega) = \frac{1}{2\pi} \sum_{k=1}^N \gamma_k \text{Re}[G_{ij}^c(i\omega_k)], \quad (7)$$

where $\{i\omega_k\}_{k=1}^N$ and $\{\gamma_k\}_{k=1}^N$ are precalculated imaginary frequency grid points and corresponding weights, respectively [44]. Knowing the density matrix, the particle number is calculated by

$$N_p = \text{Tr}[\Gamma], \quad (8)$$

where the trace Tr involves the summation over bands, k points, and spins. The particle number will be taken as an indicator of the convergence in the self-consistency.

In order to calculate the polarizability χ and self-energy Σ in real space and imaginary time, a Fourier transformation (FT) of G from imaginary frequency to imaginary time is needed. Again, direct FT of the interacting Green's function $G(i\omega)$ is ill defined. Therefore, we follow the same strategy that was used when determining the density matrix in Eq. (3). Thus, $G(i\tau)$ also comprises two parts,

$$G(i\tau) = G^{\text{HF}}(i\tau) + G^c(i\tau). \quad (9)$$

In addition, we have used the definitions of the occupied (\underline{G}) and unoccupied (\overline{G}) Green's functions as in Ref. [41], which are evaluated for negative and positive imaginary time, respectively. With \underline{G} and \overline{G} , G can be expressed as

$$G(i\tau) = \theta(-\tau) \underline{G}(i\tau) + \theta(\tau) \overline{G}(i\tau). \quad (10)$$

The evaluation of $G^{\text{HF}}(i\tau)$ is straightforward since it is diagonal in the HF canonical-orbital basis:

$$\underline{G}_{ij}^{\text{HF}}(i\tau) = \delta_{ij} e^{-(\epsilon_i^{\text{HF}} - \mu)\tau} \quad (i, j \in \text{occ}), \quad (11)$$

$$\overline{G}_{ij}^{\text{HF}}(i\tau) = -\delta_{ij} e^{-(\epsilon_i^{\text{HF}} - \mu)\tau} \quad (i, j \in \text{unocc}). \quad (12)$$

The correlated $G^c(i\tau)$ can be efficiently calculated by inverse discrete cosine and sine transformations [44]

$$\underline{G}_{ij}^c(i\tau_m) = \sum_{n=1}^N \xi_{mn} \cos(\tau_m \omega_n) \text{Re}[G_{ij}^c(i\omega_n)] - \sum_{n=1}^N \zeta_{mn} \sin(\tau_m \omega_n) \text{Im}[G_{ij}^c(i\omega_n)], \quad (13)$$

$$\overline{G}_{ij}^c(i\tau_m) = \sum_{n=1}^N \xi_{mn} \cos(\tau_m \omega_n) \text{Re}[G_{ij}^c(i\omega_n)] + \sum_{n=1}^N \zeta_{mn} \sin(\tau_m \omega_n) \text{Im}[G_{ij}^c(i\omega_n)]. \quad (14)$$

Here, $\{i\tau_m\}_{m=1}^N$ are optimized imaginary-time grid points and the coefficients ξ and ζ are precalculated and stored [41,44].

After the matrices $\underline{G}_{ij}(i\tau)$ and $\overline{G}_{ij}(i\tau)$ in the HF canonical-orbital basis have been obtained, they are transformed to the natural-orbital basis using the unitary matrix U that diagonalizes the interacting density matrix Γ in Eq. (2):

$$G_{mn}(i\tau) = \sum_{ij} [U^\dagger]_{mi} G_{ij}(i\tau) U_{jn}. \quad (15)$$

Moreover, the HF canonical orbitals $|\psi_{\mathbf{jk}}^{\text{HF}}\rangle$ are rotated to the natural orbitals as well,

$$|\psi_{m\mathbf{k}}\rangle = \sum_j U_{jm} |\psi_{\mathbf{jk}}^{\text{HF}}\rangle, \quad (16)$$

since it is more convenient to evaluate the charge density and the new HF Hamiltonian H^{HF} in the basis that diagonalizes the interacting density matrix, that is, in the natural-orbital basis.

Within the PAW method [49,50], $G_{mn}(i\tau)$ are then transformed from the natural-orbital basis to the plane-wave (PW) basis by

$$G_{\mathbf{k}}^{(1)}(\mathbf{g}, \mathbf{G}', i\tau) = \sum_{m,n} \langle \mathbf{g} | \tilde{\psi}_{m\mathbf{k}} \rangle G_{mn}(i\tau) \langle \tilde{\psi}_{n\mathbf{k}} | \mathbf{G}' \rangle, \quad (17)$$

$$G_{\mathbf{k}}^{(2)}(v, \mathbf{G}', i\tau) = \sum_{m,n} \langle \tilde{p}_v | \tilde{\psi}_{m\mathbf{k}} \rangle G_{mn}(i\tau) \langle \tilde{\psi}_{n\mathbf{k}} | \mathbf{G}' \rangle, \quad (18)$$

$$G_{\mathbf{k}}^{(3)}(\mathbf{g}, \alpha', i\tau) = \sum_{m,n} \langle \mathbf{g} | \tilde{\psi}_{m\mathbf{k}} \rangle G_{mn}(i\tau) \langle \tilde{\psi}_{n\mathbf{k}} | \tilde{p}'_{\alpha} \rangle, \quad (19)$$

$$G_{\mathbf{k}}^{(4)}(v, \alpha', i\tau) = \sum_{m,n} \langle \tilde{p}_v | \tilde{\psi}_{m\mathbf{k}} \rangle G_{mn}(i\tau) \langle \tilde{\psi}_{n\mathbf{k}} | \tilde{p}'_{\alpha} \rangle, \quad (20)$$

where $\tilde{\psi}_{n\mathbf{k}}$ are pseudo natural orbitals and \tilde{p}_μ are projectors, which are dual to the pseudo partial waves $\tilde{\phi}_\mu$ within the augmentation sphere [49,50].

Knowing $G(i\tau)$ in imaginary time, the polarizability $\chi(i\tau)$ is obtained by contraction over \underline{G} and \overline{G} in real space and imaginary time

$$\chi(i\tau) = G(i\tau) G(-i\tau) \quad (\tau > 0), \quad (21)$$

which is immediately transformed to $\chi(i\omega)$ in imaginary frequency by the cosine transformations [41,44], where the calculations of the correlated screened interactions W^c are

conveniently done using the RPA:

$$W^c(i\omega) = \epsilon^{-1}(i\omega)V - V. \quad (22)$$

Here, V is the bare Coulomb interaction kernel and the inverse of the dielectric function is calculated by

$$\epsilon^{-1}(i\omega) = 1 + V\chi^{\text{red}}(i\omega), \quad (23)$$

with the reducible polarizability χ^{red} given by

$$\chi^{\text{red}}(i\omega) = [1 - \chi(i\omega)V]^{-1}\chi(i\omega). \quad (24)$$

The $W^c(i\omega)$ is then transformed to $W^c(i\tau)$ by the inverse of cosine transformations [41,44]. Finally, the new correlated self-energy Σ^c is evaluated by the contraction of G and W^c in real space and imaginary time:

$$\Sigma^c(i\tau) = -G(i\tau)W^c(i\tau). \quad (25)$$

For the calculations of $\chi(i\tau)$ and $\Sigma^c(i\tau)$ within the PAW method, we refer the reader to our previous publication [41]. $\Sigma^c(i\tau)$ is then transformed to $\Sigma^c(i\omega)$ in the imaginary frequency domain by the cosine and sine transformations [41]. With the new $\Sigma^c(i\omega)$ and H^{HF} , the self-consistency loop of scGW is closed. This procedure is repeated until convergence is achieved.

It should be noted that in the second iteration and beyond, the correlated self-energy $\Sigma^c(i\omega)$ is always first evaluated in the natural-orbital basis and then transformed to the HF canonical-orbital basis, where an analytic continuation is performed via a Padé fit [51] to obtain the QP energies and spectral functions.

B. Head of the dielectric function

In the long-wavelength limit ($\mathbf{q} \rightarrow 0$), a special treatment needs to be done for the head of $\epsilon_{\mathbf{G},\mathbf{G}'}^{-1}(\mathbf{q}, i\omega)$ (corresponding to $\mathbf{G} = \mathbf{G}' = 0$) due to the singularity of the bare Coulomb interaction. Within G_0W_0 , this issue can be tackled through a Taylor expansion of KS one-electron energies and orbitals around $\mathbf{q} = 0$ [38–40]. It can be shown [38–40] that the KS polarizability $\chi_{0,0}^{\text{KS}}(\mathbf{q}, i\omega)$ at small \mathbf{q} for gapped systems has the behavior [52]

$$\chi_{0,0}^{\text{KS}}(\mathbf{q}, i\omega) = a\mathbf{q}^2 + b\mathbf{q}^4 + \mathcal{O}(\mathbf{q}^6), \quad (26)$$

where a and b are \mathbf{q} -independent constants that can be evaluated explicitly [38–40]. This leads to the disappearance of the divergence in $\lim_{\mathbf{q} \rightarrow 0} \epsilon_{0,0}^{-1}(\mathbf{q}, i\omega)$ because of the cancellation of the $1/\mathbf{q}^2$ terms in the bare Coulomb interaction. However, this expansion is not possible in subsequent iterations of a scGW calculation and thus a different solution is needed.

Assuming Eq. (26) holds true for the general polarizability $\chi_{0,0}(\mathbf{q}, i\omega)$, the head of ϵ^{-1} has the form

$$\epsilon_{00}^{-1}(\mathbf{q}, i\omega) = A + B\mathbf{q}^2 + \mathcal{O}(\mathbf{q}^4). \quad (27)$$

The parameters A and B are obtained from a linear least-square fit on the data from finite \mathbf{q} . The resulting fit is then extrapolated to $\mathbf{q} = 0$ to estimate the head of $\epsilon_{\mathbf{G},\mathbf{G}'}^{-1}(\mathbf{q}, i\omega)$ in the long-wavelength limit. We note that, in principle, $\lim_{\mathbf{q} \rightarrow 0} \epsilon_{0,0}^{-1}(\mathbf{q}, i\omega)$ is a tensor depending on the direction from which \mathbf{q} approaches zero, but unfortunately our proposed strategy can only approximately yield the average of diagonal

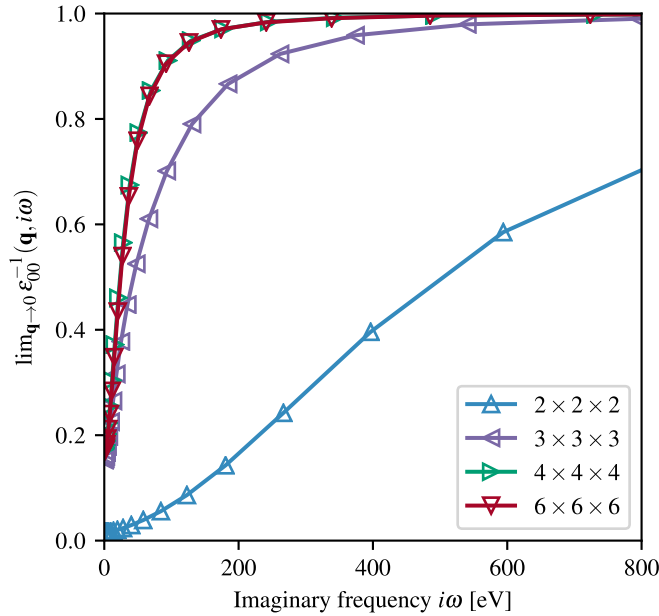


FIG. 1. k -point convergence of $\epsilon_{0,0}^{-1}(\mathbf{q}, i\omega)$ in the long-wavelength limit. The data were obtained from *scGW* calculations for diamond.

elements of the tensor. However, this makes it suitable for the cubic systems considered in this work.

In order to check this extrapolation scheme, we compared the extrapolated $\lim_{\mathbf{q} \rightarrow 0} \epsilon_{0,0}^{-1}(\mathbf{q}, i\omega)$ to the results from G_0W_0 calculations, where $\lim_{\mathbf{q} \rightarrow 0} \epsilon_{0,0}^{-1}(\mathbf{q}, i\omega)$ is available from the above-mentioned $\mathbf{k} \cdot \mathbf{p}$ perturbation theory. It was found that the extrapolated $\lim_{\mathbf{q} \rightarrow 0} \epsilon_{0,0}^{-1}(\mathbf{q}, i\omega)$ for diamond using a $6 \times 6 \times 6$ k -point grid are almost identical to the ones from perturbation theory. This justifies our extrapolation scheme and we can thus apply it to the *scGW* calculations.

The accuracy of the extrapolation scheme also depends on the k -point sampling used because higher k -point densities yield more data points in the region of small finite \mathbf{q} . As an illustration, Fig. 1 shows the convergence of $\lim_{\mathbf{q} \rightarrow 0} \epsilon_{0,0}^{-1}(\mathbf{q}, i\omega)$ of diamond with respect to k -point sampling. It can be seen that a $2 \times 2 \times 2$ k -point mesh is far from sufficient to obtain the converged head. Results from $3 \times 3 \times 3$ are improved, but still not satisfactory. Convergence seems to be achieved at $4 \times 4 \times 4$ k points and the results from $6 \times 6 \times 6$ k points are almost unchanged compared to $4 \times 4 \times 4$.

We point out here that the inclusion of the head corrections in the *scGW* calculations is important to obtain the precise QP energies and spectral functions as compared to calculations without head corrections (see the results in Sec. IV).

III. TECHNICAL DETAILS

The *scGW* method has been implemented in the Vienna *ab initio* simulation package (VASP) [53,54]. All calculations were performed using approximately norm-conserving (NC) GW PAW potentials, the details of which are given in Table I of Ref. [36]. Table I lists all the 15 semiconductors and insulators considered in this work with their respective crystal structures, lattice constants at low temperature (if

TABLE I. Crystal structures, lattice constants a , and plane-wave energy cutoffs $E_{\text{cut}}^{\text{pw}}$ for all the materials considered.

	Crystal structure	a (Å)	$E_{\text{cut}}^{\text{pw}}$ (eV)
BN	zinc blende	3.61	700.00
C	diamond	3.56	741.69
SiC	zinc blende	4.35	741.69
MgO	rock salt	4.21	821.52
GaN	zinc blende	4.53	801.99
ZnO	zinc blende	4.58	802.27
Si	diamond	5.43	609.83
AlP	zinc blende	5.46	616.62
AlAs	zinc blende	5.66	613.91
InP	zinc blende	5.86	616.62
AlSb	zinc blende	6.13	571.80
CdS	zinc blende	5.81	657.51
ZnS	zinc blende	5.40	802.27
GaP	zinc blende	5.45	801.99
InSb	zinc blende	6.47	561.76

available, otherwise at room temperature), and plane-wave energy cutoffs of the potentials, which were chosen to be the maximum of all elements in the considered material. The energy cutoff for the response function was chosen to be half of the PW cutoff. The number of bands was set to be the maximum number of PWs compatible to a given PW cutoff energy. To sample the Brillouin zone, $6 \times 6 \times 6$ k -point grids centered at the Γ point were used, unless explicitly stated otherwise. The number of imaginary-time/frequency points was set to 24 for all materials. Five *scGW* iterations were performed, which was found to be sufficient to converge the QP energies to within 0.01 eV. For comparison, independent QPGW calculations [27] were also performed with 128 real frequency points and a maximum of six iterations.

In all cases except InSb, standard KS-DFT calculations employing the Perdew-Burke-Ernzerhof (PBE) functional [55,56] were used as starting points for the *scGW* and QPGW calculations. For InSb, however, the hybrid-functional HSE06 [57,58] was used instead because in this case PBE yields an even qualitatively wrong (negative) band gap. It needs to be mentioned that the starting point (PBE or HSE06 functional) is only relevant to G_0W_0 results due to its first-order perturbative nature, whereas for *scGW* and QPGW calculations the results are independent of the starting functional.

Since the convergence of the QP energies with respect to the basis set is slow, we have exploited a basis-set correction scheme [36,37,46] using the fact that the basis-set incompleteness error $E^{\text{QP}}(\infty) - E^{\text{QP}}(N_{\text{pw}})$ decays as $1/N_{\text{pw}}$, where N_{pw} is the number of PWs. Specifically, the PW energy cutoff $E_{\text{cut}}^{\text{pw}}$ is increased by a factor of 1.25 and 1.587, leading to an increase in N_{pw} by a factor of 1.4 and 2.0, respectively. The obtained results are fitted as a linear function of $1/N_{\text{pw}}$ and then extrapolated to $1/N_{\text{pw}} = 0$ to get the final basis-set corrected QP energies. This was done for both *scGW* and QPGW calculations. Because the *scGW* and QPGW calculations are rather demanding and the basis-set corrections depend only weakly on the number of k points [36,37], the basis-set corrections were performed with $3 \times 3 \times 3$ k points.

TABLE II. Comparison of calculated scGW QP energies of diamond with and without head corrections for the dielectric function using $6 \times 6 \times 6$ k points. Note that the basis-set and k -point set corrections are not included here. ΔIP is the absolute shift of the VBM at the Γ point compared to PBE calculations. Since the changes in the density and the electrostatic potential are small from PBE to scGW, ΔIP is expected to be fairly pseudo/PAW potential independent. The other columns represent the relative position of the valence band minimum at the Γ point (Γ_{VBMmin}), the VBM at the L and X points (L_v and X_v), and the CBM at the Γ , L , and X points (Γ_c , L_c , and X_c) relative to the VBM at Γ . All values are given in eV.

	ΔIP	Γ_{VBMmin}	Γ_c	L_v	L_c	X_v	X_c
Without head	-2.47	-23.88	10.64	-3.13	13.75	-7.07	9.29
With head	-1.37	-24.55	8.46	-3.08	11.59	-6.98	7.10

The basis-set corrected QP energies at $6 \times 6 \times 6$ k points are then obtained by

$$E_{\infty}^{6 \times 6 \times 6} = E_{\text{red}}^{6 \times 6 \times 6} + E_{\infty}^{3 \times 3 \times 3} - E_{\text{red}}^{3 \times 3 \times 3}, \quad (28)$$

where $E_{\text{red}}^{6 \times 6 \times 6}$ and $E_{\text{red}}^{3 \times 3 \times 3}$ are the QP energies calculated using default energy cutoffs shown in Table I for $6 \times 6 \times 6$ and $3 \times 3 \times 3$ k points, respectively, and $E_{\infty}^{3 \times 3 \times 3}$ is the basis-set corrected QP energy. It was found that the basis-set corrections are generally small (<100 meV), except in a few cases such as ZnO where they can be as large as a few hundred meV [36,59,60].

A similar extrapolation scheme was used to correct the errors introduced by the k -point sampling under the assumption that the k -point set error behaves as $1/N_k$ with N_k being the total number of k points used. To this end, additional calculations were performed using a $4 \times 4 \times 4$ k -point mesh. The final converged QP energies including both basis-set and k -point set corrections were obtained by

$$E_{\infty}^{\infty} = E_{\infty}^{6 \times 6 \times 6} + E_{\text{red}}^{\infty} - E_{\text{red}}^{6 \times 6 \times 6}, \quad (29)$$

where the k -point corrections $E_{\text{red}}^{\infty} - E_{\text{red}}^{6 \times 6 \times 6}$ were calculated with the reduced basis set corresponding to the default PW

cutoff energy, based on the observation that the k -point corrections depend only weakly on the basis set [37]. Typically, the k -point corrections were found to be on the same order of magnitude as the basis-set corrections.

IV. RESULTS

We present our scGW results first for the selected case of diamond to show the effects of the inclusion of the head of the dielectric function obtained from the extrapolation scheme described in Sec. II B and of the self-consistency on particle number, QP energies, and spectral functions. Then, we extend our discussions to all other materials.

Table II shows a comparison of the calculated scGW QP energies for diamond at selected k points with and without the head of the dielectric function. It can be seen that inclusion of the head corrections changes the QP energies substantially, especially for deep states (see Γ_{VBMmin}) and unoccupied states (see Γ_c , L_c , and X_c). Without the head corrections, the band gap is significantly overestimated as compared to the case with the head corrections. This is more obviously seen from Fig. 2(a), where the comparison of the scGW QP band structures with and without head corrections is shown. In addition, it is found that with head corrections, the convergence of the particle number is faster than without head corrections (not shown). These findings indicate that the inclusion of the head of the dielectric function is crucial to obtain accurate and converged QP energies in scGW calculations with a reasonable k -point set.

Next, we turn to discuss the effects of self-consistency. Figure 3 shows the calculated scGW band gap and total particle number of diamond as a function of the iterations. First, it can be seen that convergence has already been achieved at the fourth iteration. The converged particle number is calculated to be 8 to an accuracy of 10^{-4} , evidencing that scGW satisfies the conservation of particle number from a numerical point of view [17,18,31]. As the number of iterations increases, the band gap increases and finally reaches the converged value of 6.41 eV up to a precision of 10 meV. We note in passing that

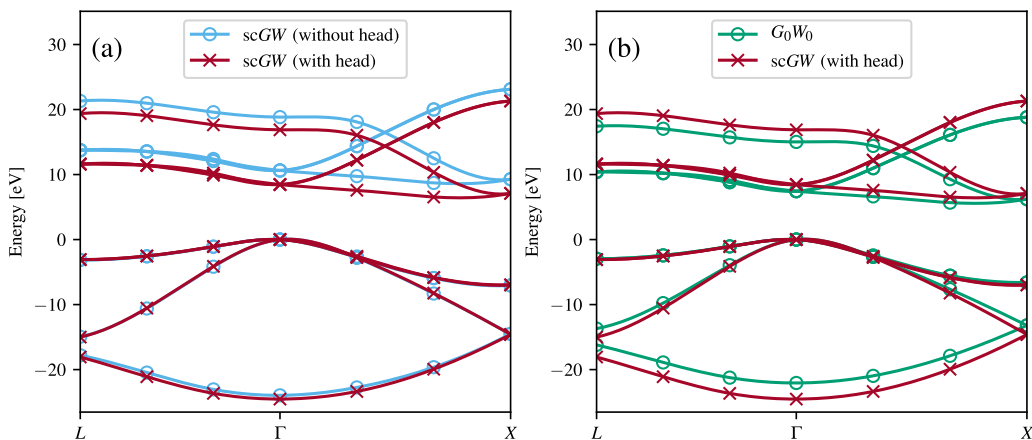


FIG. 2. (a) Comparison of the scGW QP band structure of diamond with and without head corrections in the dielectric function for $6 \times 6 \times 6$ k points. (b) scGW QP band structure with head corrections versus G_0W_0 QP band structure. The data shown here do not include basis-set corrections and k -point corrections. The VBM at the Γ point has been aligned to zero. The smooth lines were obtained using a cubic-spline interpolation.

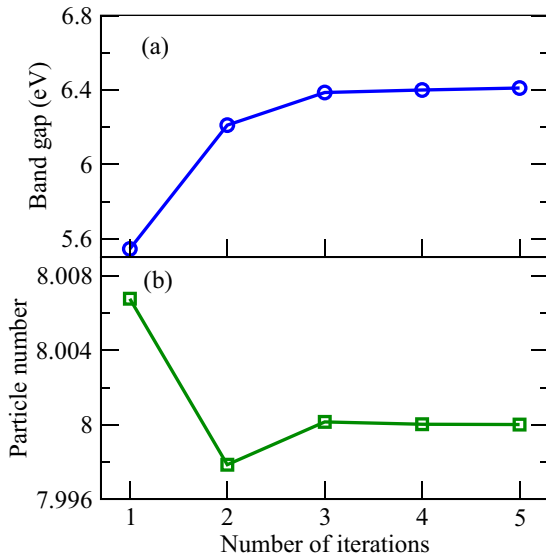


FIG. 3. Calculated (a) band gap and (b) total particle number of diamond from scGW calculations as a function of the number of iterations. The particle number was obtained from the interacting density matrix [Eq. (8)] after each iteration.

our calculated band gap is about 0.26 eV larger than the scGW result of Kutepov [13]. The discrepancy might arise from different implementation and setup details, such as potentials, basis sets, and k -point grid used. Also, it is not clear how the head of the dielectric function was dealt with in Ref. [13]. Second, one can see that the scGW band gap is significantly enlarged compared to G_0W_0 . This is more clearly seen from the QP band structure comparison between scGW and G_0W_0 in Fig. 2(b). This is expected because our full scGW does not take into account vertex corrections. Indeed, inclusion of vertex corrections in scGW will reduce the gap towards the experimental value [13,14], but this is beyond the scope of this work.

Figure 4 shows the scGW spectral functions of diamond for selected bands at the Γ point along with G_0W_0 spectral

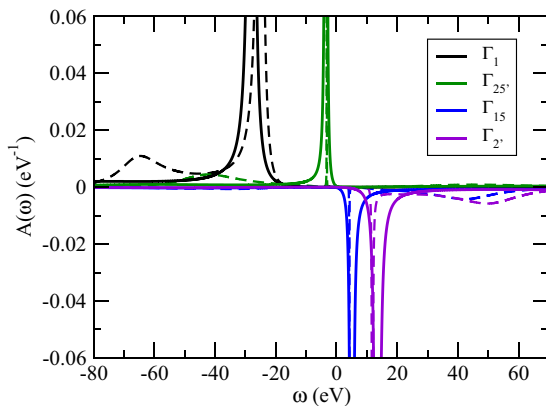


FIG. 4. Comparison of scGW (solid lines) and G_0W_0 (dashed lines) spectral functions of diamond for selected bands at Γ . Note that the signs of the spectral functions for unoccupied states such as Γ_{15} and $\Gamma_{2'}$ are intentionally reversed for clarity.

TABLE III. The renormalization factor Z of the QP peaks of diamond for selected bands at Γ predicted by G_0W_0 and scGW.

	Γ_1	$\Gamma_{25'}$	Γ_{15}	$\Gamma_{2'}$
G_0W_0	0.753	0.827	0.828	0.771
scGW	0.885	0.884	0.897	0.903

functions. One can observe that, compared to G_0W_0 , the QP peaks of the spectral functions from scGW at the Γ point are broadened and dramatically shifted up and down for unoccupied and occupied bands, respectively, leading to a significant enhancement of the direct band gap. This is consistent with the QP band structures shown in Fig. 2(b). In addition, we find that the satellite structures (plasmonic polarons) appearing far below or above the QP peaks in G_0W_0 are washed out in scGW, in accordance with the increased renormalization factor Z of QP peaks predicted by scGW (see Table III). It is known that these satellites are to some extent artifacts of the G_0W_0 approximation, although similar features are observed in x-ray photoemission experiments [8,10]. In the experiment the features are interpreted as replicas of the QP peak shifted by the typical plasmon frequency. The complete absence of these features in the scGW is troublesome and clearly suggests that one needs to go beyond the GW approximation, for example, by the cumulant expansion of the Green's function [7–11] or by including an approximate vertex.

Having validated our scGW implementation for the selected case of diamond, we now extend our discussion to all other considered materials. The calculated scGW QP energies are compiled in Table IV. For comparison, the QP energies obtained from G_0W_0 and QPGW calculations are also given in Tables V and VI, respectively. We first note that our G_0W_0 QP energies agree very well with the results in Ref. [36] with deviations less than 50 meV for all the materials

TABLE IV. QP energies and fundamental band gaps (Δ_{gap}) (in eV) from scGW calculations. The meaning of each column is the same as in Table II. Note that for InSb, Δ_{IP} is calculated with respect to HSE06 calculations.

	Δ_{IP}	Γ_{VBmin}	Γ_c	L_v	L_c	X_v	X_c	Δ_{gap}
BN	-2.02	-23.42	12.86	-2.07	13.81	-5.27	7.67	7.67
SiC	-1.28	-17.96	8.69	-1.18	7.85	-3.56	3.29	3.29
C	-1.37	-24.76	8.33	-3.06	11.47	-6.95	6.97	6.41
Si	-1.09	-15.58	4.71	-1.43	3.34	-3.48	2.29	2.18
AIP	-1.10	-13.03	5.01	-0.82	4.52	-2.26	3.20	3.20
AlAs	-1.09	-13.37	3.73	-0.87	3.75	-2.31	2.98	2.98
AlSb	-0.93	-12.74	3.18	-1.02	2.78	-2.47	2.61	2.61
InP	-0.92	-13.52	1.97	-1.04	2.89	-2.50	3.04	1.97
InSb	-0.50	-11.46	0.79	-1.00	1.40	-2.26	2.13	0.79
GaN	-1.55	-18.92	3.94	-1.01	7.19	-2.83	5.57	3.94
GaP	-0.83	-14.12	3.17	-1.11	2.96	-2.82	2.77	2.77
ZnO	-3.04	-20.06	4.92	-0.82	10.40	-2.23	9.52	4.92
ZnS	-1.72	-14.43	4.68	-0.86	6.02	-2.24	5.70	4.68
CdS	-1.60	-14.60	3.46	-0.84	5.65	-2.09	5.88	3.46
MgO	-3.27	-20.08	9.53	-0.80	12.83	-1.65	13.80	9.53

TABLE V. Same as Table IV, but for G_0W_0 results.

	Δ_{IP}	Γ_{VBmin}	Γ_c	L_v	L_c	X_v	X_c	Δ_{gap}
BN	-1.51	-20.89	11.33	-2.07	12.29	-5.17	6.39	6.39
SiC	-1.03	-15.51	7.35	-1.09	6.63	-3.29	2.42	2.42
C	-1.22	-21.98	7.44	-2.94	10.39	-6.59	6.24	5.69
Si	-0.71	-12.00	3.24	-1.21	2.10	-2.85	1.26	1.15
AIP	-0.94	-11.28	4.20	-0.78	3.77	-2.13	2.47	2.47
AlAs	-1.01	-11.71	2.97	-0.83	3.07	-2.17	2.30	2.30
AlSb	-0.84	-10.64	2.38	-0.91	2.06	-2.21	1.86	1.86
InP	-0.79	-11.15	1.26	-0.98	2.10	-2.39	2.32	1.26
InSb	-0.58	-10.88	0.57	-1.19	1.23	-2.37	1.98	0.57
GaN	-1.19	-15.31	2.87	-0.98	5.95	-2.72	4.54	2.87
GaP	-0.85	-12.28	2.62	-1.14	2.45	-2.72	2.31	2.31
ZnO	-1.77	-18.19	2.55	-0.83	7.55	-2.20	7.08	2.55
ZnS	-1.31	-11.96	3.43	-0.85	4.77	-2.20	4.66	3.43
CdS	-1.12	-11.40	2.16	-0.78	4.22	-2.01	4.59	2.16
MgO	-2.10	-17.82	7.49	-0.73	10.76	-1.48	11.78	7.49

considered except for ZnO and InSb. The deviations arise from the different implementations and setups. Specifically, our G_0W_0 QP energies were obtained from the analytic continuation of the self-energy in imaginary frequency, whereas the results of Ref. [36] were computed from the self-energy evaluated along the real frequency axis. Both methods can result in errors: the analytic continuation is known to be ill conditioned, although band gaps are usually very accurate. On the other hand, calculations along the real frequency axis are prone to discretization errors. In addition, to calculate the derivative of the cell-periodic part of the KS orbitals with respect to \mathbf{k} , $|\nabla_{\mathbf{k}}u_{n\mathbf{k}}\rangle$, which is needed to deal with the long-wavelength limit of the dielectric function [39], the finite-difference method by the perturbation expansion after discretization (PEAD) method [61] was used in this work, while in Ref. [36] $|\nabla_{\mathbf{k}}u_{n\mathbf{k}}\rangle$ was obtained by linear response theory [39]. Although both methods strictly converge to the same values when the number of k points is sufficiently large, the dielectric function converges from below and above for the PEAD and linear response, respectively. This means that the

TABLE VI. Same as Table IV, but for QPGW results.

	Δ_{IP}	Γ_{VBmin}	Γ_c	L_v	L_c	X_v	X_c	Δ_{gap}
BN	-2.25	-21.61	12.55	-2.33	13.48	-5.34	7.50	7.50
SiC	-1.35	-16.22	7.82	-1.19	7.14	-3.43	2.88	2.88
C	-1.81	-22.73	8.03	-3.08	11.20	-6.71	6.97	6.43
Si	-1.01	-12.15	3.65	-1.23	2.47	-2.93	1.60	1.49
AIP	-1.28	-11.80	4.74	-0.81	4.29	-2.23	2.94	2.94
AlAs	-1.43	-12.23	3.58	-0.85	3.62	-2.25	2.84	2.84
AlSb	-1.13	-11.02	2.78	-0.94	2.43	-2.28	2.22	2.22
InP	-1.13	-11.73	1.64	-1.01	2.53	-2.43	2.71	1.64
InSb	-0.77	-10.98	0.61	-1.05	1.31	-2.36	2.05	0.61
GaN	-1.74	-16.38	3.78	-1.02	6.91	-2.81	5.39	3.78
GaP	-1.12	-12.78	3.05	-1.18	2.86	-2.82	2.67	2.67
ZnO	-2.85	-19.02	4.29	-0.83	9.46	-2.29	8.86	4.29
ZnS	-1.80	-13.32	4.27	-0.89	5.66	-2.30	5.42	4.27
CdS	-1.65	-12.61	2.89	-0.81	4.98	-2.01	5.31	2.89
MgO	-3.42	-18.32	9.58	-0.52	12.71	-1.36	13.75	9.58

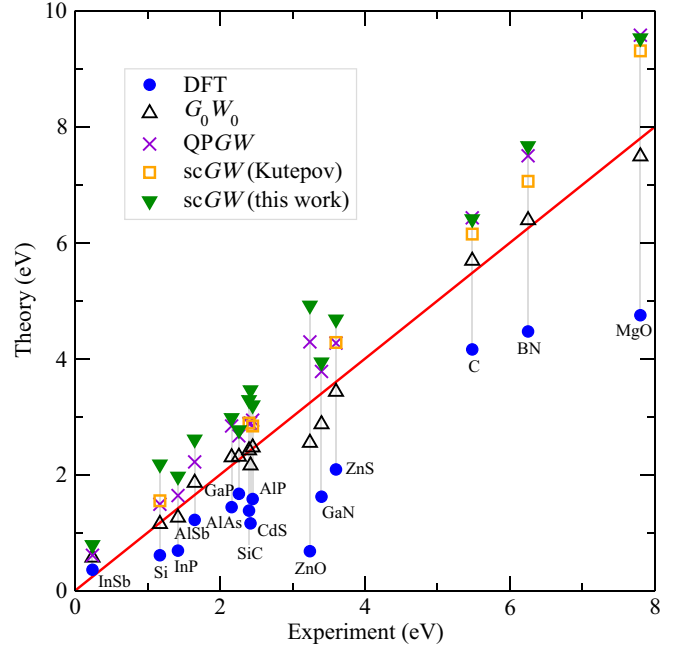


FIG. 5. Comparison of band gaps obtained from different theoretical methods and experiments for the whole set of materials considered here. The scGW results of Kutepov are taken from Ref. [13]. Experimental values are taken from Ref. [14] and references therein. Note that the HSE06 calculated band gap is shown for InSb.

band gaps converge from above and below for the PEAD and linear response, respectively. This explains the larger band gap of ZnO in our G_0W_0 calculations as compared to Ref. [36]. For the small $6 \times 6 \times 6$ k mesh used here, the PEAD method is found to be more accurate since the calculated dielectric functions are already very close to the converged values. The larger deviation for InSb is understood because our G_0W_0 calculations for InSb were done on top of the HSE06 functional instead of the PBE calculations used in Ref. [36].

We now turn to the scGW and QPGW results. scGW and QPGW raise the unoccupied states, but lower the occupied states, in particular the deep states (see Γ_{VBmin} in the tables for instance), with the shifts being more apparent in scGW. Figure 5 furthermore shows the band gaps calculated from various theoretical methods at different levels against experimental results. In addition, the scGW results for a subset of materials from Kutepov [13] are also shown for comparison. One can see that, as expected, PBE underestimates the band gaps due to neglected integer discontinuity. Inclusion of the nonlocal dynamical self-energy in the G_0W_0 approximation improves the band gaps towards the experimental values. Nevertheless, from a fundamental point, G_0W_0 is always somewhat unsatisfactory since the good agreement arises almost certainly from the aforementioned cancellation of errors due to the lack of self-consistency and vertex corrections. Introducing self-consistency only, however, deteriorates the results, leading to a significant increase of the scGW and QPGW band gaps as compared to G_0W_0 and experiment. The overestimation is generally larger in scGW than QPGW, which is due to the smaller values in the dielectric functions predicted by scGW. This shows that the RPA is not sufficiently accurate

when used on top of *scGW* or *QPGW* calculations. This was to be expected since Hedin's equations clearly imply that the interaction kernel must be set to the functional derivative of the self-energy (here $\Sigma = GW$) with respect to the Green's function G . Neglecting the variation of W with respect to G , this implies that even at the simplest level of theory, one needs to include a screened exchange interaction W via the Bethe-Salpeter equation in the irreducible polarizability.

Our calculated *scGW* band gaps are, in general, consistent with the results of Kutepov [13] for the given materials, but are a bit larger, typically by up to 0.4 eV. The possible reasons for the deviations have already been discussed before. We want to reiterate here that our *scGW* band gaps have been corrected for the finite basis-set errors as well as errors introduced by the finite k -point sampling. Also, the singularity problem associated with the long-wavelength limit of the dielectric function has been carefully dealt with by the extrapolation scheme.

V. CONCLUSIONS

To summarize, we have presented converged QP energies for 15 semiconductors and insulators from a fully self-consistent *GW* implementation within the PAW method. Converged band gaps have been obtained by including both finite basis-set corrections and k -point corrections, as well as using accurate (norm-conserving) *GW* PAW potentials. Furthermore, a simple extrapolation scheme has been used to determine the dielectric matrix in the long-wavelength limit. All implementation details were given and particular emphasis was put on the extrapolation scheme. Our implementation was tested, first by investigating the selected case of diamond and then for the entire set of compounds. The calculated *scGW* band gaps were compared to G_0W_0 , *QPGW*, and, where available, *scGW* band gaps as well as experimental results. It was found that for the *scGW* calculations the inclusion of

the head corrections in the dielectric function is important to obtain reasonably fast convergence of the QP energies.

From a physical point of view, our results can be summarized as follows. The *scGW* method yields mostly unsatisfactory results compared to experiment. Notably, the band gaps are significantly overestimated compared to experiment, and plasmonic satellites are entirely missing in the spectral function (see Fig. 4). As we have explained in the previous section, this is related to the absence of vertex corrections, which Hedin's equations dictate to be the derivative of the *GW* self-energy with respect to the external potential. As already discussed by Kutepov [12,13], including a consistent vertex is a formidable task: even in the simplest approximation, one would need to include a vertex W via the Bethe-Salpeter equation [15], which increases the compute cost by at least an order of magnitude. Worse, if one would continue self-consistency, the derivative of the self-energy [then $\Sigma = GW\Gamma$ (using a very simple Γ)] with respect to the Green's function G would create even more diagrams, increasing the complexity of the vertex further. So, one is necessarily faced with the dilemma at which level of theory one terminates the cycle. This choice will be mandated by the computational requirements and the implementational complexity. Without question, *scGW* is unsatisfactory. Nevertheless, our calculations establish accurate reference values for *scGW*, upon which one can now try to improve, for instance, by including the simplest possible vertex W .

ACKNOWLEDGMENTS

This work was supported by the FWF within the SFB ViCoM (Grant No. F 41). Supercomputing time on the Vienna Scientific cluster (VSC) is gratefully acknowledged. J.K. was supported by the European Union's Horizon 2020 research and innovation programme under the Marie Skłodowska-Curie Grant Agreement No. 658705.

-
- [1] L. Hedin, *Phys. Rev.* **139**, A796 (1965).
 - [2] L. Hedin and S. Lundqvist, *Solid State Physics* (Academic, New York, 1969).
 - [3] G. Strinati, H. J. Mattausch, and W. Hanke, *Phys. Rev. Lett.* **45**, 290 (1980).
 - [4] G. Strinati, H. J. Mattausch, and W. Hanke, *Phys. Rev. B* **25**, 2867 (1982).
 - [5] M. S. Hybertsen and S. G. Louie, *Phys. Rev. Lett.* **55**, 1418 (1985).
 - [6] M. S. Hybertsen and S. G. Louie, *Phys. Rev. B* **34**, 5390 (1986).
 - [7] F. Aryasetiawan, L. Hedin, and K. Karlsson, *Phys. Rev. Lett.* **77**, 2268 (1996).
 - [8] M. Guzzo, G. Lani, F. Sottile, P. Romaniello, M. Gatti, J. J. Kas, J. J. Rehr, M. G. Silly, F. Sirotti, and L. Reining, *Phys. Rev. Lett.* **107**, 166401 (2011).
 - [9] J. J. Kas, J. J. Rehr, and L. Reining, *Phys. Rev. B* **90**, 085112 (2014).
 - [10] F. Caruso, H. Lambert, and F. Giustino, *Phys. Rev. Lett.* **114**, 146404 (2015).
 - [11] B. Gumhalter, V. Kovac, F. Caruso, H. Lambert, and F. Giustino, *Phys. Rev. B* **94**, 035103 (2016).
 - [12] A. L. Kutepov, *Phys. Rev. B* **94**, 155101 (2016).
 - [13] A. L. Kutepov, *Phys. Rev. B* **95**, 195120 (2017).
 - [14] A. Grüneis, G. Kresse, Y. Hinuma, and F. Oba, *Phys. Rev. Lett.* **112**, 096401 (2014).
 - [15] E. Maggio and G. Kresse, *J. Chem. Theory Comput.* **13**, 4765 (2017).
 - [16] J. McClain, Q. Sun, G. K.-L. Chan, and T. C. Berkelbach, *J. Chem. Theory Comput.* **13**, 1209 (2017).
 - [17] G. Baym and L. P. Kadanoff, *Phys. Rev.* **124**, 287 (1961).
 - [18] G. Baym, *Phys. Rev.* **127**, 1391 (1962).
 - [19] F. Fuchs, J. Furthmüller, F. Bechstedt, M. Shishkin, and G. Kresse, *Phys. Rev. B* **76**, 115109 (2007).
 - [20] F. Bruneval and M. A. L. Marques, *J. Chem. Theory Comput.* **9**, 324 (2013).
 - [21] X. Zhu and S. G. Louie, *Phys. Rev. B* **43**, 14142 (1991).
 - [22] O. Zakharov, A. Rubio, X. Blase, M. L. Cohen, and S. G. Louie, *Phys. Rev. B* **50**, 10780 (1994).

- [23] M. Shishkin and G. Kresse, *Phys. Rev. B* **75**, 235102 (2007).
- [24] S. V. Faleev, M. van Schilfgaarde, and T. Kotani, *Phys. Rev. Lett.* **93**, 126406 (2004).
- [25] M. van Schilfgaarde, T. Kotani, and S. Faleev, *Phys. Rev. Lett.* **96**, 226402 (2006).
- [26] F. Bruneval, N. Vast, and L. Reining, *Phys. Rev. B* **74**, 045102 (2006).
- [27] M. Shishkin, M. Marsman, and G. Kresse, *Phys. Rev. Lett.* **99**, 246403 (2007).
- [28] C. Bhandari, M. van Schilfgaarde, T. Kotani, and W. R. L. Lambrecht, *Phys. Rev. Mater.* **2**, 013807 (2018).
- [29] B. Holm and U. von Barth, *Phys. Rev. B* **57**, 2108 (1998).
- [30] W.-D. Schöne and A. G. Eguiluz, *Phys. Rev. Lett.* **81**, 1662 (1998).
- [31] A. Stan, N. E. Dahlen, and R. van Leeuwen, *J. Chem. Phys.* **130**, 114105 (2009).
- [32] F. Caruso, P. Rinke, X. Ren, M. Scheffler, and A. Rubio, *Phys. Rev. B* **86**, 081102 (2012).
- [33] A. Kutepov, K. Haule, S. Y. Savrasov, and G. Kotliar, *Phys. Rev. B* **85**, 155129 (2012).
- [34] P. Koval, D. Foerster, and D. Sánchez-Portal, *Phys. Rev. B* **89**, 155417 (2014).
- [35] A. Gulans, *J. Chem. Phys.* **141**, 164127 (2014).
- [36] J. Klimeš, M. Kaltak, and G. Kresse, *Phys. Rev. B* **90**, 075125 (2014).
- [37] Z. Ergönenc, B. Kim, P. Liu, G. Kresse, and C. Franchini, *Phys. Rev. Mater.* **2**, 024601 (2018).
- [38] S. Baroni and R. Resta, *Phys. Rev. B* **33**, 7017 (1986).
- [39] M. Gajdoš, K. Hummer, G. Kresse, J. Furthmüller, and F. Bechstedt, *Phys. Rev. B* **73**, 045112 (2006).
- [40] J. Harl, L. Schimka, and G. Kresse, *Phys. Rev. B* **81**, 115126 (2010).
- [41] P. Liu, M. Kaltak, J. Klimeš, and G. Kresse, *Phys. Rev. B* **94**, 165109 (2016).
- [42] H. N. Rojas, R. W. Godby, and R. J. Needs, *Phys. Rev. Lett.* **74**, 1827 (1995).
- [43] M. M. Rieger, L. Steinbeck, I. White, H. Rojas, and R. Godby, *Comput. Phys. Commun.* **117**, 211 (1999).
- [44] M. Kaltak, J. Klimeš, and G. Kresse, *J. Chem. Theory Comput.* **10**, 2498 (2014).
- [45] M. Kaltak, J. Klimeš, and G. Kresse, *Phys. Rev. B* **90**, 054115 (2014).
- [46] E. Maggio, P. Liu, M. J. van Setten, and G. Kresse, *J. Chem. Theory Comput.* **13**, 635 (2017).
- [47] J. M. Tomczak, P. Liu, A. Toschi, G. Kresse, and K. Held, *Eur. Phys. J. Special Top.* **226**, 2565 (2017).
- [48] X. Wang, H. T. Dang, and A. J. Millis, *Phys. Rev. B* **84**, 073104 (2011).
- [49] P. E. Blöchl, *Phys. Rev. B* **50**, 17953 (1994).
- [50] G. Kresse and D. Joubert, *Phys. Rev. B* **59**, 1758 (1999).
- [51] G. A. J. Baker, *Essentials of Padé Approximants* (Academic, New York, 1975), Chap. 18.
- [52] Note that for metals, $\chi_{0,0}^{\text{KS}}(\mathbf{q}, i\omega) = a_0 + a\mathbf{q}^2 + b\mathbf{q}^4 + \mathcal{O}(\mathbf{q}^6)$ with $a_0 \propto \beta$, where β is the inverse of the temperature.
- [53] G. Kresse and J. Hafner, *Phys. Rev. B* **47**, 558 (1993).
- [54] G. Kresse and J. Furthmüller, *Phys. Rev. B* **54**, 11169 (1996).
- [55] J. P. Perdew, K. Burke, and M. Ernzerhof, *Phys. Rev. Lett.* **77**, 3865 (1996).
- [56] J. P. Perdew, K. Burke, and M. Ernzerhof, *Phys. Rev. Lett.* **78**, 1396 (1997).
- [57] J. Heyd, G. E. Scuseria, and M. Ernzerhof, *J. Chem. Phys.* **118**, 8207 (2003).
- [58] J. Paier, R. Hirschl, M. Marsman, and G. Kresse, *J. Chem. Phys.* **122**, 234102 (2005).
- [59] B.-C. Shih, Y. Xue, P. Zhang, M. L. Cohen, and S. G. Louie, *Phys. Rev. Lett.* **105**, 146401 (2010).
- [60] C. Friedrich, M. C. Müller, and S. Blügel, *Phys. Rev. B* **83**, 081101 (2011).
- [61] R. W. Nunes and X. Gonze, *Phys. Rev. B* **63**, 155107 (2001).